Polyaniline- and Poly(ethylenedioxythiophene)-Cellulose Nanocomposite Electrodes for Supercapacitors

Soon Yee Liew,[a] *Wim Thielemans*[a,c]* *and Darren A. Walsh*[b]*

[a] Manufacturing and Process Technologies Division, Faculty of Engineering, University of Nottingham, Nottingham NG7 2RD, UK

[b] School of Chemistry, University of Nottingham, Nottingham NG7 2RD, UK

[c] Renewable Materials and Nanotechnology Research Group,

KU Leuven Campus Kortrijk, Etienne Sabbelaan 53, 8500 Kortrijk, Belgium

* wim.thielemans@kuleuven.be

*darren.walsh@nottingham.ac.uk

Dedicated to Prof. Stephen Fletcher on the occasion of his 65th birthday

Abstract The formation and characterisation of films of polyaniline (PANI) and poly(ethylenedioxythiophene) (PEDOT) containing cellulose nanocrystals (CNXLs) from cotton are described. PANI/CNXL films were electrodeposited from a solution containing CNXLs, HCl and aniline, while PEDOT/CNXL films were electrodeposited from a solution containing CNXLs, $LiClO_4$ and ethylenedioxythiophene. In each case, incorporated of CNXLs into the electrodepositing polymer film led to the formation of a porous polymer/CNXL nanocomposite structure. The films were characterised using scanning electron microscopy, cyclic voltammetry, electrochemical impedance spectroscopy (EIS) and galvanostatic charge-discharge analysis. The specific capacitances of the nanocomposite materials were higher than those of the CNXL-free counterparts (488 F g^{-1} for PANI/CNXL; 358 F g^{-1} for PANI; 69 F g^{-1} for PEDOT/CNXL; 58 F g^{-1} for PEDOT). The durability of the PANI/CNXL film under potential cycling was slightly better than that of the CNXL-free PANI, while the PEDOT film was slightly more durable than the PEDOT/CNX film. Using electrodeposition, it was possible to form thick PANI/CNXL films, with total electrode capacitances of 2.07 F cm^{-2} (and corresponding specific capacitances of 440 F g^{-1}), demonstrating that this particular nanocomposite may be promising for the construction of high performance supercapacitors.

Keywords: supercapacitor; conducting polymer; capacitance; electrochemical impedance spectroscopy; cyclic voltammetry; porous materials

Introduction

The development of novel supercapacitors, devices that fit the gap between high energy/low power batteries and low energy/high power capacitors, is a very active area of research [1-3]. Much of this work is aimed at the design of new electrode materials that can store a lot of charge and withstand a large number of charge/discharge cycles. Candidate materials include activated carbons [4], carbon nanotubes [5], graphene [6,7], metal oxides [8], and electronically-conducting polymers (ECPs) such as polyaniline (PANI), poly(ethylenedioxythiophene) (PEDOT), and polypyrrole (PPY) [9,10]. ECPs are particularly promising as unlike, *e.g.*, carbon nanostructures that only store charge at the electrode/electrolyte interface, ECPs can store charge throughout their bulk structure due to their faradaic charging mechanism (*i.e.*, pseudocapacitance). However, a common weakness of such materials is their propensity to degrade during repeated charge/discharge cycles, when ion and solvent transfer across the ECP/electrolyte interface causes swelling and shrinkage of the ECP. This weakness is often overcome by incorporating rigid support materials such as carbon nanotubes (CNTs) into the ECPs, which can yield mechanically stable nanocomposites [10-13].

As part of a wider move towards the use of renewable materials in science and technology, a number of groups have begun to explore the use of such materials in electrochemical energy conversion and storage [14-16]. As one of the most abundant materials on Earth, cellulose (and its derivatives) has received attention as a potential fuel for electricity generation in fuel cells [17,18] and as an additive in composite electrodes for fuel cells, batteries and supercapacitors [19-22]. Cellulose has been particularly useful for the development of flexible devices [23-36] and a number of wearable cellulose-based supercapacitors have been developed [37-40].

Cellulose nanocrystals (CNXLs) are high aspect ratio, crystalline portions of cellulose that can be readily extracted from renewable plant resources using simple acid hydrolysis. CNXLs have attracted a lot of attention in recent years [41,42] and their incorporation into PPY-based composites using electrochemical co-deposition has yielded promising electrode materials for supercapacitors [43,44]. The mass-specific capacitances, C_{sp}, of nanocomposite PPY/CNXL electrodes are comparable to those of PPY/CNT nanocomposites synthesised using a similar procedure (336 F g^{-1} and 319 F g^{-1}, respectively, based on analysis by cyclic voltammetry), as are the materials' stabilities, demonstrating the opportunities offered by the inexpensive, renewable CNXLs [44]. PPY/CNXL nanocomposites with a C_{sp} of 248 F g^{-1} have also been prepared by chemical synthesis [45]. While the development of materials with high C_{sp} values is undoubtedly important and such data are encouraging, the parameter of interest in real devices is usually the total electrode capacitance, C_E, given in units of F cm^{-2} (normalised to the electrode's geometric area). The use of materials with high C_{sp} values does not necessarily translate into high capacitance devices and both C_{sp} and C_E should be considered when analysing novel supercapacitor electrode materials. For ECP-based supercapacitors, typical C_E values are of the order of 1 F cm^{-2} [46-48] and a PPY/CNXL supercapacitor with electrode capacitances of 2 F cm^{-2} and a mass specific capacitance of 240 F g^{-1} was recently reported [43].

Given the promising performances of PPY/CNXL nanocomposites, it is important to determine whether CNXLs can be used in supercapacitor electrode nanocomposites based on other ECPs. In this paper, we describe the electrochemical synthesis of PANI/CNXL and PEDOT/CNXL nanocomposite films on Pt and glassy carbon surfaces, respectively, and compare their performances against those of the corresponding CNXL-free ECPs. As we discuss below, the capacitance of each nanocomposite materials exceeds that of the CNXL-free ECP. In the case of the PANI/CNXL films, in particular, C_{sp} is 440 F g^{-1} and C_E exceeds

2 F cm^{-2}, demonstrating the opportunities afforded by the use of CNXLs in supercapacitor development.

Materials and Methods

Materials and Apparatus

The cellulose source was cotton wool. Concentrated H_2SO_4 and HCl, aniline (ANI) and TEMPO (2,2,6,6-tetra-methylpiperidine-1-oxyl) were obtained from Alfa Aesar and all other reagents were obtained from Sigma-Aldrich. All reagents were used as received. Electrochemical depositions and measurements were carried out using a model 760C potentiostat (CH Instruments Inc., Austin, TX) using either a 2 mm diameter Pt disk or a 3 mm diameter glassy carbon (GC) disk as the working electrode, an Ag/AgCl reference electrode and a Pt wire as the counter electrode. Samples for scanning electron microscopy (SEM) were prepared by electrodeposition onto GC plates (exposed area = 0.283 cm^2) and SEM analysis was carried out using a Philips XL30 FEG Environmental Scanning Electron Microscope operated at 20 kV.

Extraction and Modification of CNXLs from Cotton

CNXLs were extracted from cotton wool using a H_2SO_4 hydrolysis process described by Revol [49], which yields CNXLs with average dimensions of approximately $6 \times 6 \times 150$ nm. The preparation method also introduces a negative surface charge onto the CNXLs as some of the surface primary hydroxyl groups on the CNXLs' exteriors are converted to sulfate half esters [50,51]. During the deposition of PANI/CNXL films, the as-prepared CNXLs were used. For the deposition of PEDOT/CNXL nanocomposite films, the CNXLs were first

subjected to TEMPO oxidation, which converts the primary hydroxyls to carboxylates (these oxidised CNXLs are called O-CNXLs) [52]. Carboxylation was confirmed by potentiometric titration, giving approximately 1 mmol g^{-1} carboxylate groups on the O-CNXLs, as expected from previous work [44,52].

Electrochemical Measurements

Prior to use, Pt and GC electrodes were cleaned by polishing with aqueous alumina (0.3 μm) slurries on felt polishing pads and then rinsing with deionized water. For the electrodeposition of the PANI/CNXL films, deposition solutions contained 0.25 M ANI in a 0.5 wt.% CNXL suspension in 0.5 M HCl. CNXL-free PANI films were electrodeposited from 0.25 M ANI dissolved in 1.0 M HCl. PEDOT/O-CNXL films were deposited from 38 mM EDOT in a solution composed of 5 parts 50 mM $LiClO_4$ in a 0.79 wt.% O-CNXL dispersion and 2 parts CH_3CN. Pure PEDOT films were deposited from solutions composed of 38 mM EDOT in 5 parts 100 mM $LiClO_4$ and 2 parts CH_3CN. PANI and PANI/CNXL films were electrodeposited at +0.9 V *vs*. Ag/AgCl whereas PEDOT and PEDOT/O-CNXL films were electrodeposited at +1.1 V *vs*. Ag/AgCl. The optimum deposition potential was determined using cyclic voltammetry (full details are given in the Results and Discussion section). After deposition, the electrodes were gently rinsed with de-ionised water. The electrochemical properties of the PANI and PANI/CNXL films were studied in 1.0 M HCl and the PEDOT and PEDOT/O-CNXL films were characterised in 2.0 M KCl. Electrodeposition and electrochemical characterisation of all materials were performed at room temperature (~ 20˚C).

Results and discussion

Electrochemical Deposition of PANI/CNXL and PEDOT/CNXL Nanocomposites

Figure 1 shows cyclic voltammograms (CVs) recorded at (A) a Pt electrode in ANI and ANI/CNXL solutions and (B) a GC electrode in EDOT and EDOT/O-CNXL solutions. In each case, monomer oxidation began near 0.8 V and a nucleation loop appeared, indicating that nucleation and growth of the ECPs occurred during the forward sweep and that deposition during the reverse sweep occurred preferentially on the pre-existing polymer [53-55]. Based on the oxidation potentials shown in these CVs, subsequent PANI and PANI/CNXL films were synthesised at a constant potential of 0.9 V, while PEDOT and PEDOT/O-CNXL films were synthesised at +1.1 V, allowing us to avoid over-oxidation of the films while also enabling good control of the deposition charge [44,46].

Figure 2 shows SEM images of PANI, PANI/CNXL, PEDOT and PEDOT/O-CNXL films on electrode surfaces. The morphology of the PANI film (Figure 2A) is similar to that previously reported for electrodeposited PANI [46,56]. By comparison, the PANI/CNXL composite film had a more open structure and contained rectilinear structures consistent with those expected for polymer-coated CNXLs [44]. From the SEM images, the average pore size in the PANI film was estimated to be approximately 100 nm, while the average pore size in the PANI/CNXL film was approximately 400 nm. It is generally believed that the formation of more open ECP structures by incorporation of nanomaterials such as CNXLs and CNTs improves solvent and ion transport throughout ECP films and improves their electrochemical properties [43,44,46]. In the case of the PEDOT systems, the effects of the O-CNXLs on the polymer morphology was more evident than that observed in the PANI systems. The O-CNXL-free PEDOT film contained relatively thick aggregates, as expected

for electrodeposited PEDOT [46,48], but the PEDOT/O-CNXL film (Figure 2D) was porous, which again is expected to improve the electrochemical performance of the nanocomposite.

Electrochemical Characterisation of PANI and PANI/CNXL Films

Figure 3A shows CVs recorded at a PANI/CNXL film and a PANI film in 1.0 M HCl after a stable response was obtained for both the films. In general, both CVs had the rectangular shapes expected for predominently capacitive responses and the sharp current decreases at the potential limits were due to fast redox switching within the polymer films [57]. It is notable that the PANI/CNXL film exhibited a higher average current and a more rapid current decrease at the positive limit. As the CNXLs used during electrodeposition of PANI/CNXL films were uncharged (the surface sulfate half esters will be protonated during electrodeposition in 0.5 M HCl and during characterisation in 1 M HCl), these differences in electrochemical behaviour are thought to be due only to the structural differences in the PANI systems. This behaviour is unlike that observed in the PPY/O-CNXL system [44] and the PEDOT/O-CNXL system (*vide infra)*, which is affected by the surface charge of the O-CNXLs. Considering only the structural differences in the PANI and PANI/CNXL structures, and the fact that during potential cycling of the PANI film the accompanying ion ingress/egress can cause distortion of the film [58], it is possible to elucidate the advantages offered by the PANI/CNXL. As ECP films swell during ion ingress some of the interconnected pores within the films can become blocked increasing the barrier to subsequent ion ingress. In this scenario, the PANI/CNXL composite holds a significant advantage as the more open porous structure of the PANI/CNXL can allow more swelling and ion transport and maintenance of this open porous structure was possible due to the structural reinforcement offered by the rigid CNXL scaffold.

The effect of the facilitated ions transport in the PANI/CNXL film can be further examined through the use of electrochemical impedance spectroscopy (EIS). As a steady state, dynamic frequency technique with a small potential variation, EIS can provide a more accurate estimate of the capacitance [46]. More importantly, EIS also allows easy comparison of the charge transfer dynamics of various films by determining the 'knee' frequency from Nyquist plots or by comparing real impedance values. Figure 3B shows Nyquist plots obtained from EIS of PANI and PANI/CNXL films. Both films showed typical diffusive-capacitive behaviour from high to low applied frequency. In the high frequency region (above the knee frequency - towards the left of the *x*-axis), the pseudocapacitive behaviour of the film was limited ion diffusion into/out of the film within the time frame of the frequency period. In the low frequency region (below the knee frequency - the vertical section of the Nyquist plot), the film becomes completely charged. Thus, the knee frequency is the highest frequency where the film can be fully charged. The knee frequency of the PANI/CNXL nanocomposite was 37 Hz (at 10 ohms real impedance), compared to 21 Hz (at 14 ohms real impedance) for the PANI film. The significantly higher knee frequency and lower real impedance value as measured on the *x*-axis of the nanocomposite film indicates that charging of the PANI/CNXL film can occur at much faster rate than in the PANI film [44].

In the low frequency domain, where the film showed capacitive behaviour characterised by the near vertical Nyquist plot, the capacitance, C, of the films were determined using the equation $C = -1/(2\pi f Z'')$, where f = frequency (Hz) and Z'' = imaginary component of the complex impedance in ohms at frequency f. At 0.12 Hz, C for the PANI/CNXL film was 1.45 mF and that of the PANI film was 1.06 mF. Converting these values to C_{sp} values (considering the mass of PANI only) gives a value of 488 F g^{-1} for the PANI/CNXL composite (exceeding that of the PPY/CNXL composites described previously

[44,45]) and 358 F g^{-1} for the PANI film. Based on this analysis, together with the CV data and structural information from the SEM images, the higher capacitance and significant improvement on the charge kinetics of the PANI/CNXL nanocomposite is attributed to the porous and open-structured morphology of the nanocomposite. The high capacitances of conducting polymer/carbon nanotube (CNT) and polypyrrole/CNXL composites have also been attributed to similar morphological effects [44,46].

Electrochemical Characterisation of PEDOT and PEDOT/CNXL Films

Figure 4A shows the CVs recorded at PEDOT and PEDOT/O-CNXL films. In general, the CVs showed the rectangular shapes expected for predominantly capacitive behaviour and the CVs overlapped except in the negative potential region, where a lower current flowed at the PEDOT film. The low current at negative potentials was due to the high resistance of the reduced PEDOT [46] but, in the case of the PEDOT/O-CNXL film, the large and immobile negatively charged CNXLs within the nanocomposite film led to a high current at negative potentials [44]. This is due to electrostatic repulsion of electrons on the PEDOT chain by the negatively-charged O-CNXLs, which makes electron removal easier and results in the observed negative shift of the oxidation potential [44,46]. The Nyquist plots recorded at -0.6 V (when the films are reduced - Figure 4B) showed that the PEDOT/O-CNXL film was much more capcitive than the PEDOT film (as characterised by the more vertical plot). At 0.6 V, when the films are oxidised, the Nyquist plots almost overlap demonstrating that the films behave similarly at high potentials (Figure 4C). The bending of the Nyquist plots at high frequencies (particularly visible in Figure 4C) is unusual for ECP materials. It is thought that this phenomenon is most likely due to experimental artefacts, both capacitive and inductive, that are inherent to the use of the potentiostat [59]. The low frequency capacitance calculated

from EIS data recorded at 0 V (data not shown), where the average current was observed in the CVs (Figure 4A) and 0.045 Hz, was 69 F g^{-1} for the PEDOT/O-CNXL film and 58 F g^{-1} for the PEDOT film.

Effects of Potential Cycling on the Electrochemical Behaviour of ECP Films

Figure 5A shows galvanostatic charge/discharge curves recorded at a PANI film and a PANI/CNXL film at 1.0 mA cm^{-2}. The near symmetrical shape of the complete charge/discharge cycle for both films shows that both exhibited almost completely capacitive behaviour within the potential limits. The longer time taken for the PANI/CNXL film to complete the charge/discharge cycle was due to the higher capacitance of the film, as capacitance $C = I/(\mathrm{d}E/\mathrm{d}t)$, where I is the constant applied current and $\mathrm{d}E/\mathrm{d}t$ is the potential scan rate. Figure 5B shows the charge/discharge curves recorded, under the same conditions, after 5000 potential cycles between 0.2 V and 0.8 V in HCl. After potential cycling, the time required to complete the charge/discharge cycles reduced significantly for both films due to film degradation, which results in loss of capacitance. In both cases, the capacitance loss was gradual throughout the 5000 potential cycles (see supplementary information). It is clear from Figure 5B that the capacitance of the PANI/CNXL film was higher than that of the PANI film at the end of the stability test. The capacitance of the PANI/CNXL film had decreased by 51 % compared to 55% for the PANI film, showing that the presence of CNXLs slightly improved the electrochemical stability of PANI.

Figure 5C shows the charge/discharge curves at current density of 10 mA cm^{-2} for the PEDOT film and the PEDOT/O-CNXL film. The charge/discharge curves show that the PEDOT/O-CNXL film was also more capacitive than the PEDOT film, in agreement with the EIS discussed in the previous section. After cycling the potential 5000 times between 0.7 V

and -0.7 V, the capacitance of both films had decreased (Figure 5D). However, in this case the PEDOT/O-CNXL degraded slightly more than the PEDOT film, by 22% compared to 15%. This increased degradation may be due to the higher capacitance of the PEDOT/CNXL film. During the stability test, more ion and solvent ingress would to be expected to have occurred in the higher capacitance film (*i.e.*. the PEDOT/CNXL film) and the film would, therefore, be subjected to more mechanical stress than the PEDOT film. Similar behaviour has also been observed during potential cycling of a PEDOT/CNT nanocomposite, where the capacitance loss over a 5000-cycle potential cycling test was higher than that of a pure PEDOT film [46].

Behaviour of ECP Films Electrodeposited at High Charge Density

If one intends to use novel electrode materials in the development of real supercapacitors, the mass specific capacitance reported when only a small amount of material is used is not a reliable indicator of performance because it does not translate to device capacitance [46-48]. As Peng and co-workers pointed out previously, a good supercapacitor electrode material not only requires a high mass specific capacitance, but very importantly, it has to demonstrate a proportional increase of the electrode capacitance when a large amount of the material is used [46]. The measurement of interest in this case is the total electrode capacitance, with units of F cm^{-2}. In previous work with PPY/CNXL, a total electrode capacitance of 2.0 F cm^{-2} was achieved [43] and the challenge for the present work is to achieve similar total electrode capacitance values.

To obtain a high electrode specific capacitance, it is necessary to be able to form a porous ECP or ECP composite in order to facilitate electrolyte access throughout the volume of the material [46-48,57]. In the case of the ECP/CNXL nanocomposites, it is important to

verify that the porous structure can be retained in thick films. Figure 6A shows slow scan rate CVs (at 0.02 V s^{-1}) recorded at a PANI film and a PANI/CNXL film after electrodeposition to a charge density of 10 C cm^{-2} (*i.e.*, 50 times the charge used to form the PANI/CNXL films discussed in previous sections). The CV recorded using the PANI/CNXL film showed vertical current increases at the potential limits due to the fast charging capability of the PANI/CNXL film. This behaviour is in contrast to that observed for the PANI film, when current switch was sluggish. Differences in the charging rate were even more obvious when CVs were recorded at higher scan rates (Figure 6B shows CVs recorded at 0.25 V s^{-1}). At the higher scan rate, the PANI/CNXL film still produced a near rectangular response, suggesting that the film was highly capacitive. In contrast, the PANI film did not respond to fast charging and the slope of the CV indicates that it was resistive. Using the CVs recorded at 0.02 V s^{-1}, the capacitances of the films were calculated using the equation $C = I_{CV}/(dE/dt)$, where I_{CV} is the average current during cyclic voltammetry, and dE/dt is the potential scan rate. C_{sp} and C_E of the thick PANI/CNXL film were 440 F g^{-1} and 2.07 F cm^{-2}, respectively, while those of the thick PANI film were 285 F g^{-1} and 1.34 F cm^{-2}, respectively. C_{sp} for the thick PANI/CNXL film agrees with that obtained for the thin films (440 F g^{-1} vs 488 F g^{-1}), showing a proportional increase of electrode capacitance at higher deposition charge density. In addition, C_{sp} for the film is higher than that achieveable using PPY as the ECP [44,45]. In contrast to the PPY/CNXL film, C_{sp} of PANI decreased from 358 F g^{-1} for the thin film to 285 F g^{-1} for the thick film. The proportional increase in the capacitance of the PANI/CNXL composite is attributed to the strength of the CNXLs within the structure, which may have facilitated the retention of the porous structure in the thicker film.

Figure 6C shows the EIS Nyquist plots for the thick PANI and PANI/CNXL films. The knee frequency for the thick PANI/CNXL film was 5.5 Hz compared to 0.3 Hz for the PANI film, demonstrating that the thick PANI/CNXL film can be charged much faster than

the PANI film (as also indicated by the CVs shown in Figures 6A and 6B). It is also possible to deduce the representative pore structure in the thick PANI/CNXL and PANI films by comparing the Nyquist plots with those calculated for different typical pore structures [60]. The impedance of the thick PANI/CNXL film is characteristic of straight open pores, while that of the thick PANI film is characteristic of narrow-necked quasi-spherical pores that allow limited electrolyte access [60]. This is consistent with the SEM images that were obtained for these films (Figure 2A and 2B) and the suggestion above that the rigid CNXLs may be able to facilitate the growth of a thick porous structure in which the pores are open and interconnected.

Numerous attempts to form the PEDOT/O-CNXL films at a high deposition charge density were performed and all were unsuccessful. The PEDOT/O-CNXL films deposited to a charge density of 10 C cm^{-2} had a thick gel-like appearance when removed from the deposition solution, and displayed a poor voltammetric response. We believe this may be due to the water/acetonitrile mixture used as the deposition solution, in which the EDOT monomers and the CNXL may be preferentially dissolved/dispersed in separate phases in the mixture even though the solution appeared to consist of a single-phase [12,46]. Similar effects have been reported during the attempted formation of thick PEDOT/CNT nanocomposites (which were unsuccessful) [12,46].

Conclusions

Cellulose nanocrystals (CNXLs) from cotton were used for the electrochemical synthesis of composites with polyaniline (PANI) and poly(ethylenedioxythiophene) (PEDOT). CNXLs were incorporated into the nanocomposites during electrochemical deposition of the conducting polymers. Both CNXL nanocomposites showed higher capacitances and higher

charge/discharge rates than their CNXL-free counterparts due to the change in the polymer morphology upon forming polymer/CNXL composites, which facilitates ion and solvent transport throughout the film structure. The PEDOT/O-CNXL nanocomposite was capacitive at negative potentials where pure PEDOT was resistive, a phenomenon that we attribute to the negative charge on the immobilised O-CNXLs. Thick PANI/CNXL nanocomposites formed at high deposition charges also exhibited almost-ideal capacitive behaviour and were highly responsive to fast charging, while the CNXL-free PANI film was much more resistive when subjected to the same tests. Not only was the thick PANI/CNXL film significantly more capacitive, the rate of charge transfer in the thick PANI/CNXL film was significantly higher than in the thick PANI film. The ability to form an extended porous structure in the PANI/CNXL films (with excellent electrochemical properties) at high deposition charge is attributed to the strength of the CNXLs and the ability of the film to support facile ion and solvent movement. While there has been a couple of previous reports on high performance supercapacitor materials prepared using CNXLs as the composite filler (and polypyrrole as the ECP) [43-45], to the best of our knowledge this is the first time that such materials have been prepared using either PANI or PEDOT. This work further highlights the opportunities offered by CNXLs for the fabrication of conducting polymer composites for supercapacitor applications and extends the range of electrochemical materials that can exploit these unique nanomaterials.

Acknowledgements

We thank the UK Engineering and Physical Sciences Research Council (EPSRC) for funding this work through the DICE (Driving Innovation in Chemistry and Chemical Engineering) Project under the Science and Innovation Award (Grant Number

EP/D501229/1). SYL thanks the University of Nottingham for a Dean of Engineering International Research Scholarship and Professor Stephen Fletcher for helpful discussions on impedance artefacts.

Figure Legends

Fig. 1 (A) CVs recorded at a 2 mm-diameter Pt disk in 0.25 M ANI in 1 M HCl (black line) and in 0.25 M ANI in a 0.5 wt % CNXL dispersion in 0.5 M HCl (red line). (B) CVs recorded at a 3 mm-diameter GC disk in 38 mM EDOT in 5:2 aqueous 100 mM $LiClO_4$/acetonitrile (black line) and in 38 mM EDOT in 5:2 aqueous 50 mM $LiClO_4$ in 0.79 wt. % CNXL suspension/acetonitrile (red line). The potential scan rates and ranges were (A) 0.1 V s^{-1} and 0.2-1.0 V, and (B) 0.05 V s^{-1} and 0.2-1.2 V

Fig. 2 SEM images of (A) PANI, (B) PANI/CNXL, (C) PEDOT, and (D) PEDOT/O-CNXL films. The films in A and B had been electrodeposited at 0.9 V to a charge density of 0.2 C cm^{-2} and those in C and D had been electrodeposited at 1.1 V to a charge density of 1.0 C cm^{-2}

Fig. 3 (A) CVs recorded at an electrodeposited PANI film (black line) and a PANI/CNXL film (red line) in 1.0 M HCl. In each case, the potential was scanned from 0.2 V (initial potential) to 0.8 V at 0.25 V s^{-1}. (B) Nyquist plots obtained from EIS of the PANI film (filled circles) and the PANI/CNXL film (filled squares) at applied potential of 0.6 V in 1.0 M HCl at a potential amplitude of 5 mV and in the frequency range 0.1-10000 Hz. The knee frequency was 21 Hz for the PANI film and 37 Hz for the PANI/CNXL film. Each film had been electrodeposited at 0.9 V to a charge density of 0.2 C cm^{-2}

Fig. 4 (A) CVs recorded at an electrodeposited PEDOT film (black line) and a PEDOT/O-CNXL film (red line) in 2.0 M KCl. In each case, the potential was scanned from -0.7 V (initial potential) to 0.7 V and the scan rate was 0.25 V s^{-1}. B and C shows Nyquist plots obtained from EIS of the PEDOT/O-CNXL film (filled squares) and the PEDOT film (filled circles) at (B) -0.6 V and (C) 0.6 V in 2.0 M KCl at a potential amplitude of 5 mV and in the frequency range 0.1-10000 Hz. Each film had been electrodeposited at 1.1 V to a charge density of 1.0 C cm^{-2}

Fig. 5 Galvanostatic charge-discharge curves recorded at a PANI film (black line) and a PANI/CNXL film (red line) at a current density of 1 mA cm^{-2} (A) before and (B) after a stability test, in which the potential was cycled 5000 times between 0.2 V and 0.8 V in 1.0 M HCl at 0.05 V s^{-1}. The films were deposited at 0.9 V to a charge density of 0.2 C cm^{-2}. The curves in C and D are galvanostatic charge-discharge curves recorded at a PEDOT film (black line) and a PEDOT/O-CNXL film (red line) and films at a current density of 10 mA cm^{-2} (C) before and (D) after a stability test, in which the potential was cycled 5000 times between 0.7 V and -0.7 V in 2.0 M KCl at 0.25 V s^{-1}. The films had been electrodeposited at 1.1 V to a charge density of 1.0 C cm^{-2}

Fig. 6 (A and B) CVs recorded at an electrodeposited PANI/CNXL film (red lines) and a PANI film (black lines) in 1 M HCl. The potential limits were 0.2 V and 0.8 V and the scan rate was (A) 0.02 V s^{-1} and (B) 0.2 V s^{-1}. (C) Nyquist plots obtained from EIS of the PANI/CNXL film (squares) and the PANI film (circles) at 0.6 V in 1 M HCl at a potential amplitude of 5 mV and frequency range of 0.1-10000 Hz. The knee frequencies were 0.3 Hz

for the PANI film and 5.5 Hz for the PANI/CNXL film. Each film had been electrodeposited at 0.9 V to a charge density of 10 C cm^{-2}

References

1. Simon P and Gogotsi Y (2008) Nat. Mater. 7:845-854
2. Kotz R and Carlen M (2000) Electrochim. Acta 45:2483-2498
3. Fletcher S, Black VJ and Kirkpatrick I (2014) J. Solid State Electrochem. 18:1377-1387
4. Frackowiak E (2007) Phys. Chem. Chem. Phys. 9:1774-1785
5. Futaba DN, Hata K, Yamada T, Hiraoka T, Hayamizu Y, Kakudate Y, Tanaike O, Hatori H, Yumura M and Iijima S (2006) Nat. Mater. 5:987-994
6. Wang Y, Shi Z, Huang Y, Ma Y, Wang C, Chen M and Chen Y (2009) J. Phys. Chem. C 113:13103-13107
7. Zhu Y, Murali S, Stoller MD, Ganesh KJ, Cai W, Ferreira PJ, Pirkle A, Wallace RM, Cychosz KA, Thommes M, Su D, Stach EA and Ruoff RS (2011) Science 332:1537-1541
8. Augustyn V, Simon P and Dunn B (2014) Energy Environ. Sci. 7:1597-1614
9. Wang G, Zhang L and Zhang J (2012) Chem. Soc. Rev. 41:797-828
10. Frackowiak E, Khomenko V, Jurewicz K, Lota K and Beguin F (2006) J. Power Sources 153:413-418
11. Wu MQ, Snook GA, Gupta V, Shaffer M, Fray DJ and Chen GZ (2005) J. Mater. Chem. 15:2297-2303
12. Peng C, Snook GA, Fray DJ, Shaffer MSP and Chen GZ (2006) Chem. Commun. 4629-4631

13. Chen GZ, Shaffer MSP, Coleby D, Dixon G, Zhou WZ, Fray DJ and Windle AH (2000) Adv. Mater. 12:522-526

14. Hasani-Sadrabadi MM, Dashtimoghadam E, Nasseri R, Karkhaneh A, Majedi FS, Mokarram N, Renaud P and Jacob KI (2014) J. Mater. Chem. A 2:11334-11340

15. Chen H, Armand M, Demailly G, Dolhem F, Poizot P and Tarascon J-M (2008) Chemsuschem 1:348-355

16. Chen H, Armand M, Courty M, Jiang M, Grey CP, Dolhem F, Tarascon J-M and Poizot P (2009) J. Am. Chem. Soc. 131:8984-8988

17. Ren Z, Ward TE and Regan JM (2007) Environ. Sci. Technol. 41:4781-4786

18. Sugano Y, Vestergaard Md, Yoshikawa H, Saito M and Tamiya E (2010) Electroanalysis 22:1688-1694

19. Li J, Lewis RB and Dahn JR (2007) Electrochem. Solid-State Lett. 10:A17-A20

20. Guilminot E, Fischer F, Chatenet M, Rigacci A, Berthon-Fabry S, Achard P and Chainet E (2007) J. Power Sources 166:104-111

21. Bockenfeld N, Jeong SS, Winter M, Passerini S and Balducci A (2013) J. Power Sources 221:14-20

22. Jabbour L, Destro M, Gerbaldi C, Chaussy D, Penazzi N and Beneventi D (2012) J. Mater. Chem. 22:3227-3233

23. Nyholm L, Nystrom G, Mihranyan A and Stromme M (2011) Adv. Mater. (Weinheim, Ger.) 23:3751-3769

24. Nystrom G, Razaq A, Stromme M, Nyholm L and Mihranyan A (2009) Nano Lett. 9:3635-3639

25. Weng Z, Su Y, Wang DW, Li F, Du JH and Cheng HM (2011) Advanced Energy Materials 1:917-922

26. Zheng GY, Hu LB, Wu H, Xie X and Cui Y (2011) Energy Environ. Sci. 4:3368-3373

27. Kang YJ, Chun SJ, Lee SS, Kim BY, Kim JH, Chung H, Lee SY and Kim W (2012) ACS Nano 6:6400-6406

28. Yuan LY, Yao B, Hu B, Huo KF, Chen W and Zhou J (2013) Energy Environ. Sci. 6:470-476

29. Razaq A, Nyholm L, Sjodin M, Stromme M and Mihranyan A (2012) Adv. Energy Mater. 2:445-454

30. Kang YR, Li YL, Hou F, Wen YY and Su D (2012) Nanoscale 4:3248-3253

31. Zhang XD, Lin ZY, Chen B, Sharma S, Wong CP, Zhang W and Deng YL (2013) Journal of Materials Chemistry A 1:5835-5839

32. Liu LL, Niu ZQ, Zhang L, Zhou WY, Chen XD and Xie SS (2014) Adv. Mater. (Weinheim, Ger.) 26:4855-4862

33. Yuan L, Xiao X, Ding T, Zhong J, Zhang X, Shen Y, Hu B, Huang Y, Zhou J and Wang ZL (2012) Angewandte Chemie International Edition 51:4934-4938

34. Wang H, Zhu E, Yang J, Zhou P, Sun D and Tang W (2012) J. Phys. Chem. C 116:13013-13019

35. Pushparaj VL, Shaijumon MM, Kumar A, Murugesan S, Ci L, Vajtai R, Linhardt RJ, Nalamasu O and Ajayan PM (2007) Proc. Natl. Acad. Sci. U. S. A. 104:13574-13577

36. Gui Z, Zhu HL, Gillette E, Han XG, Rubloff GW, Hu LB and Lee SB (2013) ACS Nano 7:6037-6046

37. Niu Q, Gao K and Shao Z (2014) Nanoscale 6:4083-4088

38. Zhu L, Wu L, Sun Y, Li M, Xu J, Bai Z, Liang G, Liu L, Fang D and Xu W (2014) Rsc Advances 4:6261-6266

39. Bao LH and Li XD (2012) Adv. Mater. (Weinheim, Ger.) 24:3246-3252

40. Liang GJ, Zhu LG, Xu J, Fang D, Bai ZK and Xu WL (2013) Electrochim. Acta 103:9-14

41. Dufresne A (2013) Materials Today 16:220-227

42. Habibi Y, Lucia LA and Rojas OJ (2010) Chem. Rev. 110:3479-3500

43. Liew SY, Walsh DA and Thielemans W (2013) Rsc Advances 3:9158-9162

44. Liew SY, Thielemans W and Walsh DA (2010) J. Phys. Chem. C 114:17926-17933

45. Wu X, Chabot VL, Kim BK, Yu A, Berry RM and Tam KC (2014) Electrochim. Acta 138:139-147

46. Peng C, Jin J and Chen GZ (2007) Electrochim. Acta 53:525-537

47. Hughes M, Chen GZ, Shaffer MSP, Fray DJ and Windle AH (2002) Chem. Mater. 14:1610-1613

48. Snook GA, Peng C, Fray DJ and Chen GZ (2007) Electrochem. Commun. 9:83-88

49. Elazzouzi-Hafraoui S, Nishiyama Y, Putaux JL, Heux L, Dubreuil F and Rochas C (2008) Biomacromolecules 9:57-65

50. Araki J, Wada M, Kuga S and Okana T (1999) Journal of Wood Science 45:258-261

51. Araki J, Wada M, Kuga S and Okano T (1998) Colloids Surf., A 142:75-82

52. Habibi Y, Chanzy H and Vignon MR (2006) Cellulose 13:679-687

53. Deng ZP, Stone DC and Thompson M (1997) Analyst 122:1129-1138

54. Alves CR, Herrasti P, Ocon P, Avaca LA and Otero TF (2001) Polym. J. (Tokyo, Jpn.) 33:255-262

55. Zhao ZS and Pickup PG (1996) J. Electroanal. Chem. 404:55-60

56. Gupta V and Miura N (2006) Mater. Lett. 60:1466-1469

57. Frackowiak E and Beguin F (2001) Carbon 39:937-950

58. Yan H, Tomizawa K, Ohno H and Toshima N (2003) Macromol. Mater. Eng. 288:578-584

59. Fletcher S (2001) Electrochem. Commun. 3:692-696

60. Macdonald DD (2006) Electrochim. Acta 51:1376-1388

Figure 1

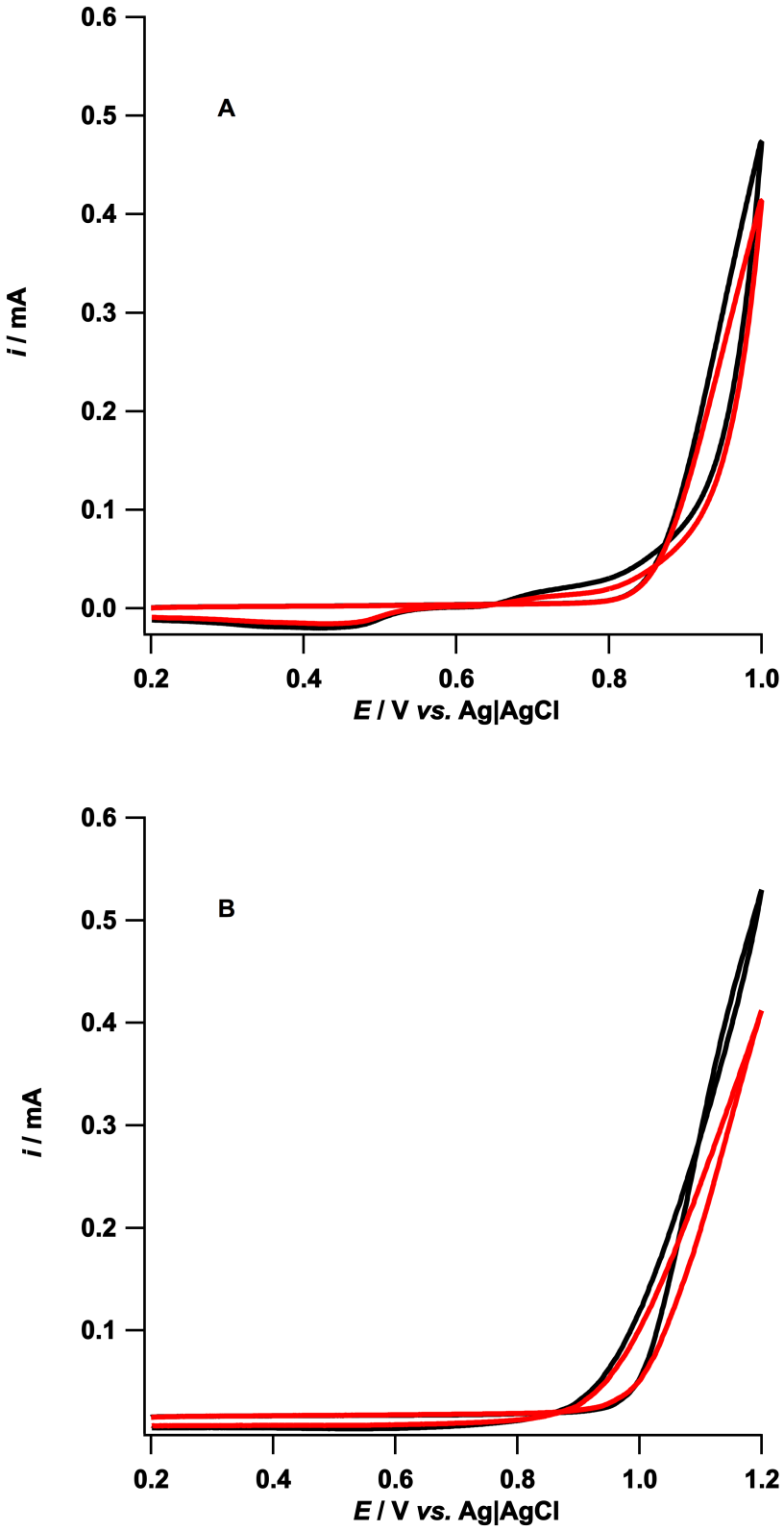

Figure 2

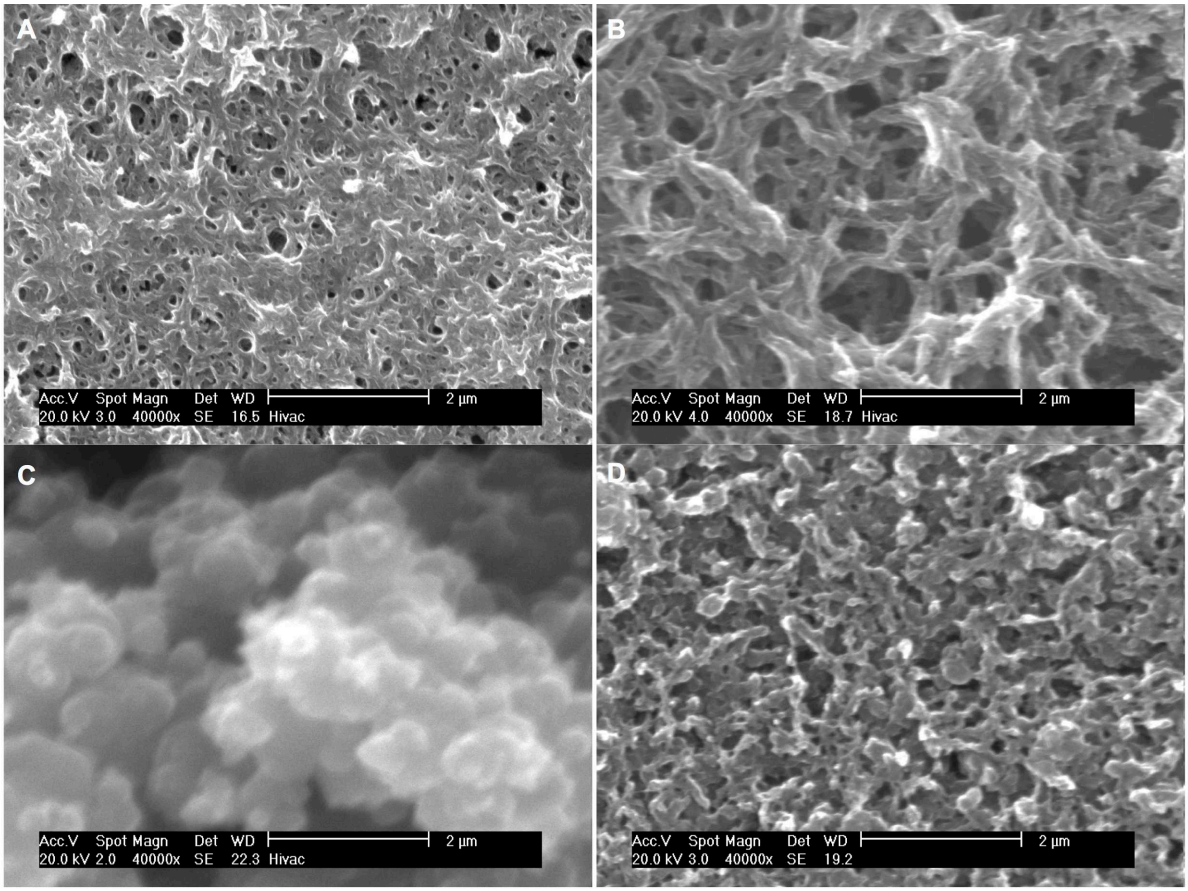
A
Acc.V Spot Magn Det WD 2 µm
20.0 kV 3.0 40000x SE 16.5 Hivac
B
Acc.V Spot Magn Det WD 2 µm
20.0 kV 4.0 40000x SE 18.7 Hivac
C
Acc.V Spot Magn Det WD 2 µm
20.0 kV 2.0 40000x SE 22.3 Hivac
D
Acc.V Spot Magn Det WD 2 µm
20.0 kV 3.0 40000x SE 19.2

Figure 3

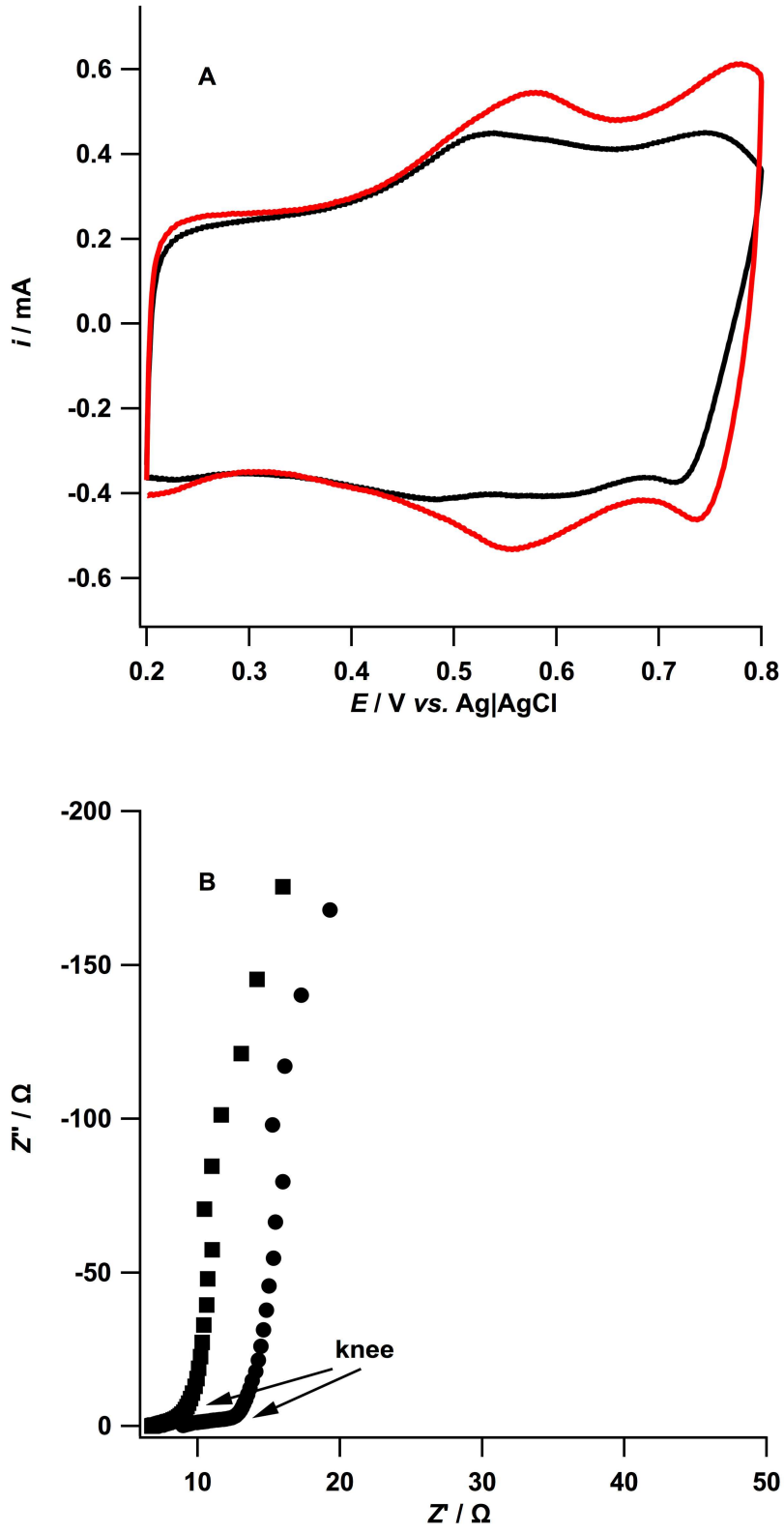
A
0.6
0.4
0.2
0.0
-0.2
-0.4
-0.6
i / mA
0.2
0.3
0.4
0.5
0.6
0.7
0.8
E / V vs. Ag|AgCl
B
-200
-150
-100
-50
0
Z'' / Ω
knee
10
20
30
40
50
Z' / Ω

Figure 4

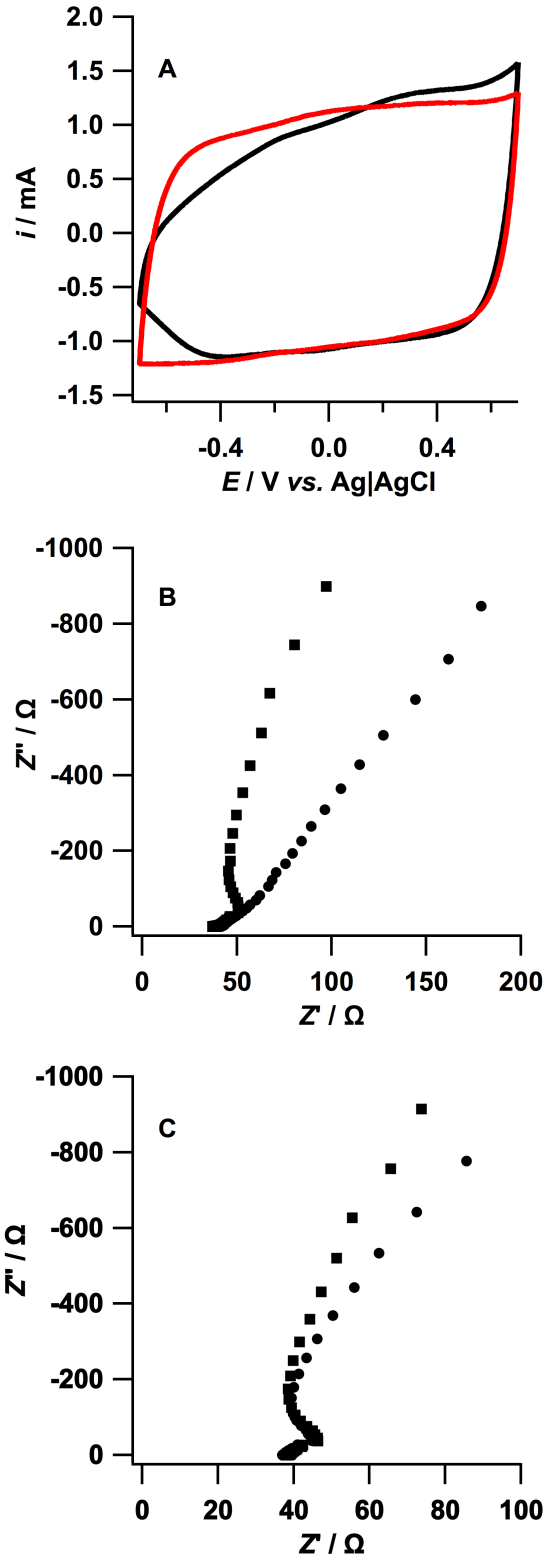
A
2.0
1.5
1.0
0.5
0.0
-0.5
-1.0
-1.5
i / mA
-0.4
0.0
0.4
E / V vs. Ag|AgCl
B
-1000
-800
-600
-400
-200
0
Z'' / Ω
0
50
100
150
200
Z' / Ω
C
-1000
-800
-600
-400
-200
0
Z'' / Ω
0
20
40
60
80
100
Z' / Ω

Figure 5

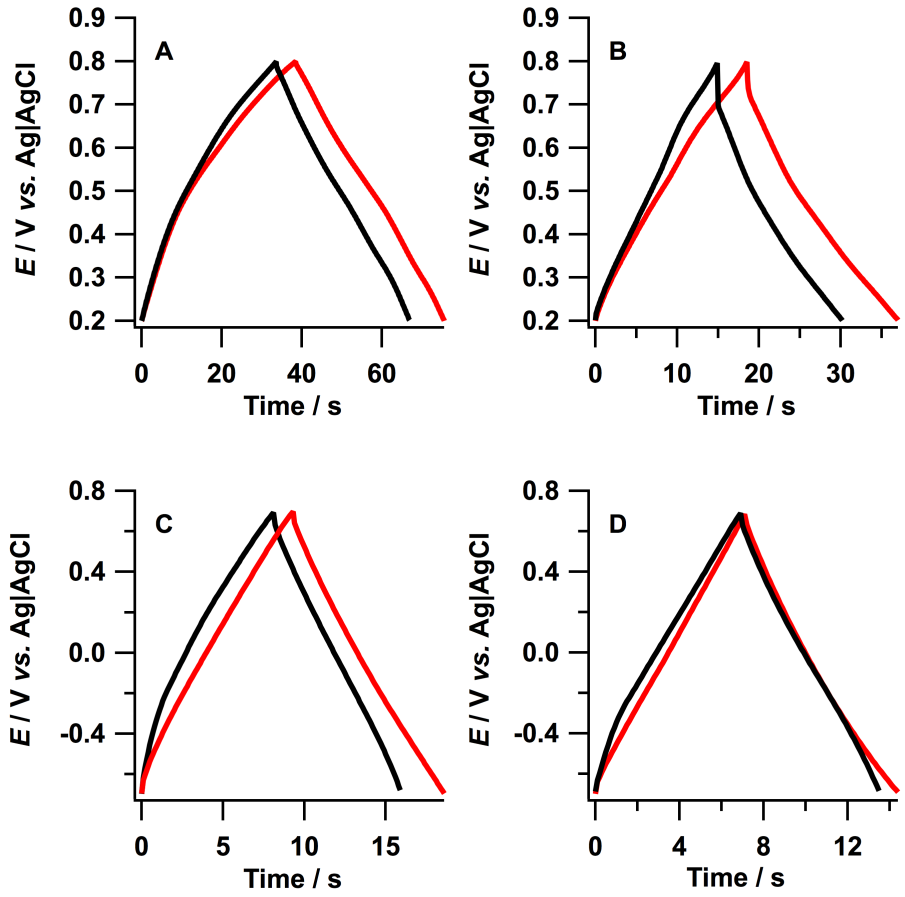
A
B
C
D
E / V vs. Ag|AgCl
Time / s
0.9
0.8
0.7
0.6
0.5
0.4
0.3
0.2
0.0
-0.4
0
20
40
60
10
30
5
15
4
8
12

Figure 6

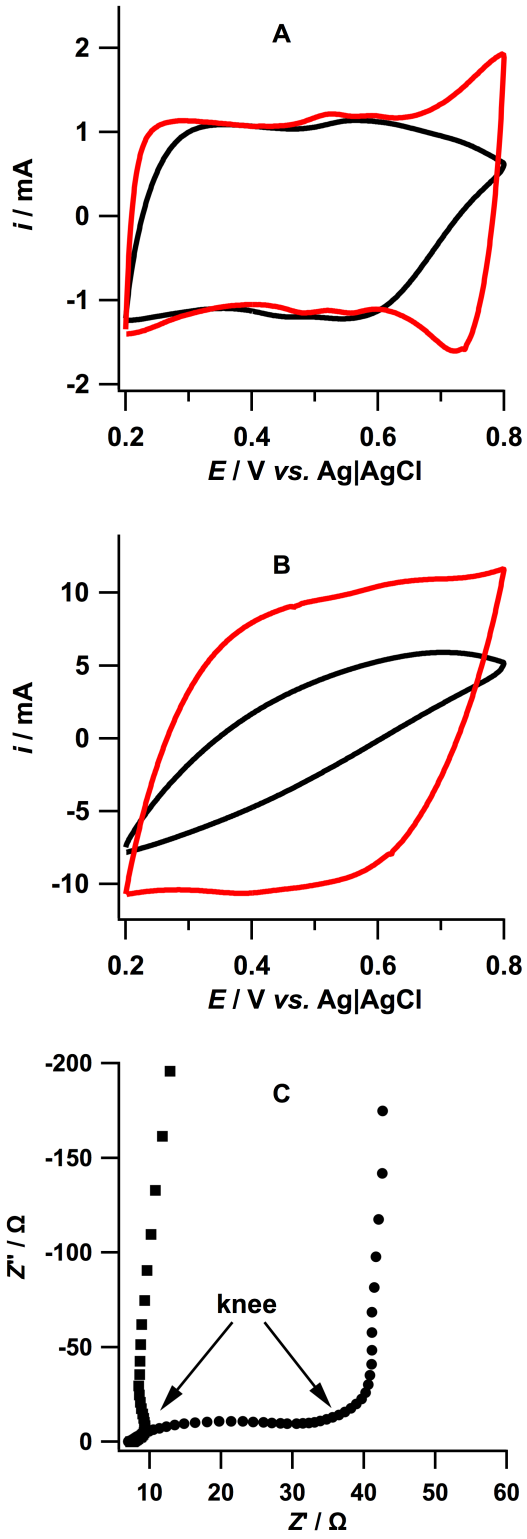
A
2
1
0
-1
-2
i / mA
0.2
0.4
0.6
0.8
E / V vs. Ag|AgCl
B
10
5
0
-5
-10
i / mA
0.2
0.4
0.6
0.8
E / V vs. Ag|AgCl
C
-200
-150
-100
-50
0
Z'' / Ω
knee
10
20
30
40
50
60
Z' / Ω